

# Evaluation of Temperature Associated Cracking in Asphalt Mixtures by Means of Performance-Based Laboratory Testing

M. Spiegl<sup>1</sup>, M. Wistuba<sup>1</sup>, R. Lackner<sup>2</sup> & R. Blab<sup>1</sup>

*Christian Doppler Laboratory of "Performance-based Optimization of Flexible Road Pavements", Vienna University of Technology, Austria.*

<sup>1</sup> *Institute for Road Construction and Maintenance, Vienna University of Technology, Austria*

<sup>2</sup> *Institute for Mechanics of Materials and Structures, Vienna University of Technology, Austria*

**ABSTRACT:** In this paper, new test methods for identification of low-temperature failure of asphalt are proposed. Low-temperature failure occurs when the stresses induced by restrained thermal shrinkage during cooling periods exceeds the tensile strength at the respective temperature. In order to specify test methods describing both (i) these in-service conditions of flexible pavements and (ii) the underlying thermorheological behavior of asphalt, the four tests characterized by different thermal and mechanical loading are required:

1. The Tensile-Stress-Restrained-Specimen Test (TSRST) is used to simulate the in-service conditions of asphalt by restraining the deformation, while the temperature is reduced by a pre-specified cooling rate;
2. The Uniaxial-Tensile-Strength Test (UTST) provides insight into the material resistance (tensile strength) at selected temperatures;
3. The Thermal-Shrinkage Test (TST) is used to specify the loading during cooling by determining the thermal shrinkage coefficient as a function of temperature; and, finally,
4. Creep/Relaxation Tests (CTs/RTs) for identification of the viscoelastic behavior of asphalt at different temperatures.

In fact, the combination of all four tests is required to fully characterize the low-temperature behavior of asphalt when subjected to thermal and mechanical (tensile) loading. Based on the obtained experimental results, key material parameters for ranking asphalts with regard to their low-temperature performance are critically reviewed. Moreover, the different test results provide important insight for the development of material models for analysis-based prediction tools and enable the formulation of optimization parameters of low temperature characteristics for mix design.

**KEY WORDS:** low-temperature behavior, thermal cracking, performance-based testing, tensile stress restrained specimen test

## 1 MOTIVATION

Two types of low-temperature cracks are observed in asphalt road pavements, i.e., regular transversal cracks caused by extreme cooling rates at very low temperatures and, secondly, longitudinal top-down cracks initiating from the pavement surface, which result from superimposed temperature- and traffic-induced stresses. In severe climates, such as e.g. in

Austria, where minimum air temperatures of  $-34\text{ }^{\circ}\text{C}$  and air-temperature cooling rates up to  $7.5\text{ }^{\circ}\text{C/h}$  are reported in long-term meteorological observations (Wistuba, 2002), opening of these two types of cracks may be caused by *one* single temperature drop.

For the assessment of the risk of low-temperature cracking of asphalt, experimental data from the TSRST and the UTST are standardly combined. Hereby, the TSRST is used to simulate temperature-induced loading within flexible pavements by reducing the temperature by a pre-specified constant cooling rate while restraining the deformation. The UTST, on the other hand, is employed to determine the material resistance (tensile strength) at different temperatures. The difference between the stress obtained from the TSRST at a certain temperature and the respective material resistance given by the UTST is referred to as tensile strength reserve  $\Delta\beta$  (Figure 1), commonly used to rank the low-temperature performance of asphalt mixtures (see, e.g., (Arand et al., 1984)). However, as regards the combination of two experiments characterized by different temperature and loading histories (TSRST and UTST) for determination of the tensile strength reserve  $\Delta\beta$ , the following questions should be addressed:

- How good is the reproducibility of experimental data? Taking the tensile loading conditions of both tests (TSRST and UTST) into account, with the test results strongly depending on the homogeneity of the asphalt material, the scatter of experimental results becomes a crucial issue.
- How do changes of test parameters (cooling rate for TSRST and strain rate for UTST) influence the experimental results?
- Is a comparison of data obtained from tests characterized by different mechanical conditions (in general, the strain rate of the UTST is by the factor 1000 higher than the thermal strain rate associated with cooling during the TSRST) and different thermal conditions (isothermal for UTST and non-isothermal for TSRST) physically sound?

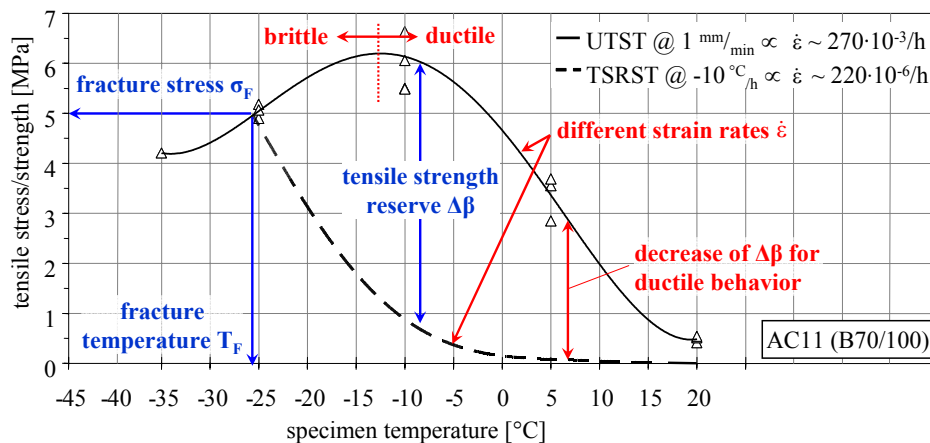


Figure 1: Determining the tensile strength reserve from TSRST and UTST.

In this paper, the tensile-strength-reserve concept, employing exclusively TSRST and UTST data, is critically reviewed by providing answers to the aforementioned questions. For this purpose, the thermal/mechanical behavior of asphalt is studied by additional experiments, such as thermal-shrinkage tests (TSTs) and creep/relaxation tests (CTs/RTs). The different test methods, the test parameters, and the expected results are outlined in the following section.

## 2 METHODS

### 2.1 Tests and Test Parameters

While the TSRST is used to simulate the in-service situation, considering temperature changes as monitored by meteorological observation, the interpretation and, later on, the derivation of key material parameters describing the low-temperature performance requires understanding of the different contributions to the mechanical deformations of asphalt, influencing the stress history measured during the TSRST. For this purpose, each one of the additional tests employed in the present study focuses on one specific type of material behavior:

- *Thermal-shrinkage behavior:* The coefficient of thermal shrinkage ( $\alpha_T$ ) is determined from TSTs. Hereby, the temperature of the asphalt sample is reduced under stress-free conditions, while its length is continuously monitored. This test is performed prior to other tests which require cooling of the asphalt sample to a certain target temperature, giving  $\alpha_T$  as a function of the temperature. For this test, a cooling rate of 10 °C/h is specified, with the cooling rate representing the only test parameter of the TST.
- *Viscous behavior:* In contrast to the TSRST and the TST, CTs are conducted under isothermal conditions (+5, -5, -15, and -25 °C). These tests are performed in three steps: first, the specimen is cooled to the test temperature (stress-free). Thereafter, a stress increment is applied. In the third step, the stress is kept constant and the strain history is monitored. In order to avoid fracture of the specimen, the maximum applied stress does not exceed 30% of the tensile strength of asphalt at the respective temperature. Parameters for the CT are the test temperature and the applied (constant) load.
- *Strength:* The tensile strength of asphalt is determined from UTSTs. Similar to the CT, this test is conducted at a specified temperature (+20, +5, -10 and -25 °C). After stress-free cooling of the asphalt specimen to the test temperature, a constant displacement rate, usually 1 mm/min, is applied. Thus, the parameters for the UTST are the test temperature and the displacement rate (FGSV, 1994).
- *Elastic behavior:* In order to determine the elastic response of asphalt, RTs are performed. Using the viscous properties identified from the CTs, the stress relaxation during RTs provides insight into the material stiffness. For the RTs, a strain increment is applied and, thereafter, kept constant while the stress is monitored. Similar to the CTs, the test parameters of the RT are the testing temperature and the applied (initial) load.

### 2.2 Test Equipment and Specimen Preparation

In order to eliminate errors arising from the use of different test equipments, all experiments described in the previous subsection are performed using one test equipment recently installed at the Christian-Doppler Laboratory (CDL) for “Performance-Based Optimization of Flexible Road Pavements”, Vienna. This electromechanical test equipment consists of a load frame, a screw jack, a computer data acquisition and control system, a climate chamber, a temperature controller, 4 linearly variable differential transducers (LVDTs), and a specimen-alignment stand (see Figure 2). The temperature in the climate chamber can be adjusted within  $T = \pm 40$  °C (accuracy of  $\pm 0.5$  °C). The LVDTs are placed outside of the climate chamber (accuracy of 0.2%), in order to eliminate influences of temperature changes on the LVDT data.

The load frame allows mounting of cylindrical and prismatic specimens. The experimental results presented in this paper were obtained from prismatic specimens (length x width x height = 225 x 50 x 50 mm). They are obtained from cutting asphalt plates (length x width x height = 500 x 260 x 50 mm) manufactured with a segment roller compactor. Two weeks after preparation, the specimens are glued onto steel adaptors and two days later they are ready for testing.

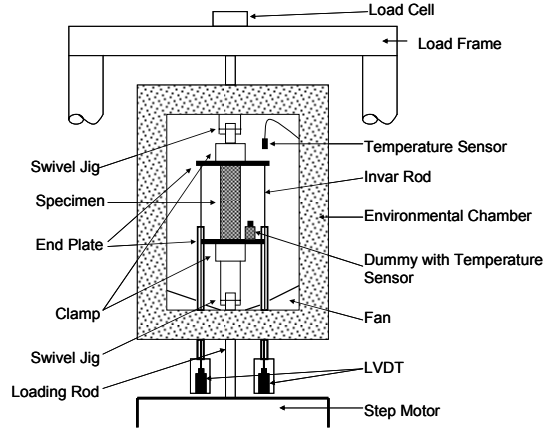


Figure 2: Illustration of setup of the employed test equipment at the CDL (Spiegel et al. 2005).

### 3 MATERIALS

Two types of asphalt commonly used in Austria for the construction of wearing courses were considered in the experimental program (see Table 1): hot mix asphalt AC-11 (maximum grain size of 11 mm) and a noise-absorbing stone-mastic asphalt SMA-11L (maximum grain size of 11 mm). For the latter, two binder materials, bitumen 50/70 and SBS polymer-modified bitumen (pmB 50-90S), were considered.

Table 1: Properties of asphalts considered in the experimental program.

asphalt	constituent	real-mass density [kg/m <sup>3</sup> ]	mass-%	voids [vol-%]	characterization
AC-11-M1	bitumen 70/100	1012	5.0	3	standard bitumen filler (calcite, dolomite) aggregate (mica, quartz, hornblende)
	limestone dust	2710	10.7		
	Loja	2847	84.3		
SMA-11L-M1	bitumen 50/70	1015	5.7	11	standard bitumen additive (cellulose fiber) filler (calcite, dolomite) aggregate (basalt)
	Viatop 80+		0.4		
	limestone dust	2710	4.8		
SMA-11L-M2	Klöch	2925	89.1	11	SBS polymer-modified bitumen additive (cellulose fiber) filler (calcite, dolomite) aggregate (basalt)
	pmB 50-90S	1018	5.5		
	Viatop 80+	2710	5.2		
	limestone dust	2710	5.2		
	Klöch	2925	88.9		

### 4 RESULTS AND DISCUSSION

The different tests performed within the experimental program are listed in Table 2. In addition to the test parameters, the bulk density and the volume fractions which, in general, vary from specimen to specimen, are provided. The volume fractions for the aggregate and the bitumen are computed from the real-mass densities and the mass fractions given in Table

1, with (vol-%) = (mass-%) x (bulk density)/(real-mass density). The difference between the volume fractions for the aggregates and the bitumen and 100% is assigned to the volume fraction of air voids.

Table 2: Test and specimen information.

sample	asphalt	test(s) performed	test parameter(s) (par. 1; par. 2)	bulk density [kg/m <sup>3</sup> ]	volume fraction of			area [mm <sup>2</sup> ]	length [mm]
					aggregate [vol-%]	bitumen [vol-%]	voids [vol-%]		
K001B	AC-11-M1	TST/UTST	-10°C; 1.0mm/min	2549.9	85.6	12.6	1.8	2600.9	224.5
K001E	AC-11-M1	TST/UTST	-10°C; 1.0mm/min	2550.0	85.6	12.6	1.8	2545.2	225.4
K001F	AC-11-M1	TST/UTST	-10°C; 1.0mm/min	2550.0	85.6	12.6	1.8	2465.1	225.6
K001C	AC-11-M1	TST/UTST	-25°C; 1.0mm/min	2551.2	85.6	12.6	1.8	2565.0	225.0
K001D	AC-11-M1	TST/UTST	-25°C; 1.0mm/min	2555.4	85.8	12.6	1.6	2580.6	225.1
K002D	AC-11-M1	TST/UTST	-25°C; 1.0mm/min	2551.8	85.7	12.6	1.7	2540.2	225.0
K002G	AC-11-M1	TSRST	10°C/h	2537.7	85.2	12.5	2.3	2494.8	225.5
K001G	AC-11-M1	TSRST	10°C/h	2542.2	85.3	12.6	2.1	2489.9	225.7
K002C	AC-11-M1	TSRST	10°C/h	2548.7	85.6	12.6	1.9	2565.4	225.0
110D	AC-11-M1	TSRST	5°C/h	2509.0	84.2	12.4	3.4	2535.1	200.7
109B	AC-11-M1	TSRST	5°C/h	2525.0	84.8	12.5	2.6	2545.2	201.6
109C	AC-11-M1	TSRST	5°C/h	2526.0	84.8	12.5	2.7	2557.8	201.7
109E	AC-11-M1	RT	5°C; 2.5kN	2521.0	84.6	12.6	2.9	2514.0	200.3
K003B	AC-11-M1	RT	-10°C; 4.0kN	2584.7	86.8	12.8	0.5	2564.6	225.3
112C	AC-11-M1	RT	-15°C; 4.0kN	2553.0	85.7	12.6	1.7	2458.9	199.0
K031G	AC-11-M1	RT	-25°C; 3.5kN	2498.7	83.9	12.4	3.8	2600.9	224.0
K030E	AC-11-M1	CT	-10°C; 2.5kN	2490.7	83.6	12.3	4.1	2627.8	223.0
K030F	AC-11-M1	CT	5°C; 1.5kN	2482.4	83.3	12.3	4.4	2622.6	223.0
K033F	AC-11-M1	CT	-15°C; 2.5kN	2513.9	84.4	12.4	3.2	2506.5	224.2
K033E	AC-11-M1	CT	-25°C; 2.5kN	2521.6	84.7	12.5	2.9	2489.1	224.2
K029C	AC-11-M1	TST/UTST	-10°C; 0.1mm/min	2531.0	85.0	12.5	2.5	2517.2	224.0
K029G	AC-11-M1	TST/UTST	-10°C; 0.1mm/min	2525.8	84.8	12.5	2.7	2560.2	223.9
K033H	AC-11-M1	TST/UTST	-25°C; 0.1mm/min	2495.8	83.8	12.3	3.9	2465.3	224.5
K030D	AC-11-M1	TST/UTST	-25°C; 0.1mm/min	2492.0	83.7	12.3	4.0	2622.6	223.6
K009D	SMA-11L-M1	TST/UTST	-10°C; 1.0mm/min	2409.2	74.1	13.5	12.3	2457.1	225.6
K007F	SMA-11L-M1	TST/UTST	-10°C; 1.0mm/min	2397.1	74.2	13.5	12.4	2466.7	224.8
K008F	SMA-11L-M1	TST/UTST	-10°C; 1.0mm/min	2405.8	74.6	13.5	11.9	2465.7	225.8
K009H	SMA-11L-M1	TST/UTST	-25°C; 1.0mm/min	2422.7	74.9	13.6	11.5	2536.0	225.0
K008B	SMA-11L-M1	TST/UTST	-25°C; 1.0mm/min	2404.1	74.7	13.5	11.8	2608.1	227.3
K009E	SMA-11L-M1	TSRST	10°C/h	2403.6	74.0	13.5	12.6	2438.5	225.2
K007C	SMA-11L-M1	TSRST	10°C/h	2404.3	74.1	13.5	12.4	2527.5	224.6
K017C	SMA-11L-M2	TST/UTST	-10°C; 1.0mm/min	2331.2	75.8	12.6	11.6	2625.3	225.0
K017D	SMA-11L-M2	TST/UTST	-10°C; 1.0mm/min	2335.3	75.9	12.6	11.4	2596.4	225.0
K016B	SMA-11L-M2	TST/UTST	-10°C; 1.0mm/min	2322.6	75.5	12.5	11.9	2519.0	224.8
K017E	SMA-11L-M2	TST/UTST	-25°C; 1.0mm/min	2340.9	76.1	12.6	11.2	2612.7	224.9
K016C	SMA-11L-M2	TST/UTST	-25°C; 1.0mm/min	2340.1	76.1	12.6	11.3	2565.9	225.0
K016D	SMA-11L-M2	TSRST	10°C/h	2336.7	76.0	12.6	11.4	2565.4	225.0
K016F	SMA-11L-M2	TSRST	10°C/h	2325.8	75.6	12.6	11.8	2502.0	224.5

Whereas the output of the performed experiments are (i) the change in distance between the top and the bottom steel adapter,  $u(t)$ , measured by the four LVDTs, and (ii) the applied load  $F(t)$ , the presentation of results reported in this section is based on the strain and stress component in the direction of loading, determined from

$$\text{strain}(t) = \frac{u(t)}{L_0} = \frac{u_1(t) + u_2(t) + u_3(t) + u_4(t)}{4L_0} \quad \text{and} \quad \text{stress}(t) = \frac{F(t)}{A_0}, \quad (1)$$

where  $L_0$  and  $A_0$  are the specimen length and cross-section area in the undeformed configuration (see Table 2). In Equation (1),  $u_i(t)$  refers to the displacement monitored by the  $i$ -th LVDT.

#### 4.1 Results from Thermal-Shrinkage Tests (TSTs)

In order to specify the amount of loading in road pavements during cooling periods, the thermal shrinkage coefficient was determined for the three considered asphalt mixtures, with the obtained strain being equal to the thermal shrinkage strain, with  $\text{strain}(t) = \varepsilon^T(t) = \alpha_T (T -$

$T_0$ ), where  $T_0$  represents the initial temperature. Thus, derivation of the strain history with respect to the temperature  $T$  gives access to the thermal shrinkage coefficient  $\alpha_T = d\varepsilon^T/dT$ . Figure 3 shows the thermal shrinkage coefficient  $\alpha_T$  for the considered asphalt mixtures. From the obtained results, the following conclusion can be drawn:

- In the temperature range from  $-15\text{ }^\circ\text{C}$  to  $0\text{ }^\circ\text{C}$ , the values for  $\alpha_T$  for all considered asphalt mixtures are approximately  $0.023\text{ mm/m/}^\circ\text{C}$  (see (Olard 2003) for similar results). The difference in the void ratio between AC-11-M1 (3 vol-%) and SMA-11L-M1 (11 vol-%) does not affect the thermal shrinkage coefficient, a fact well-known from micromechanical models developed for determination of dilation/shrinkage coefficients of multi-composed materials (see, e.g., (Pichler et al. 2003)).
- The decrease of the thermal shrinkage coefficient as the temperature approaches  $-25\text{ }^\circ\text{C}$  is similar for AC-11-M1 and SMA-11L-M1, both having standard bitumen as binder material. For the SMA-11L-M2, on the other hand, this trend is not observed, which can be explained by low-temperature characteristics of the employed pmB.
- Whereas the decrease of the thermal shrinkage coefficient in the negative temperature regime was related to the binder material, the rather low values for the shrinkage coefficient at above-zero temperatures result from the employed test equipment. Since TSTs are performed prior to UTSTs, the asphalt sample is fully mounted in the loading frame. Accordingly, any slight delay in the displacement adjustment of the test equipment required to provide stress-free conditions induces tensile stresses and, thus, results in the development of creep deformations. In the positive temperature regime, these creep deformations reduce the monitored displacements and, hence, lead to the observed underestimation of the thermal shrinkage coefficient.

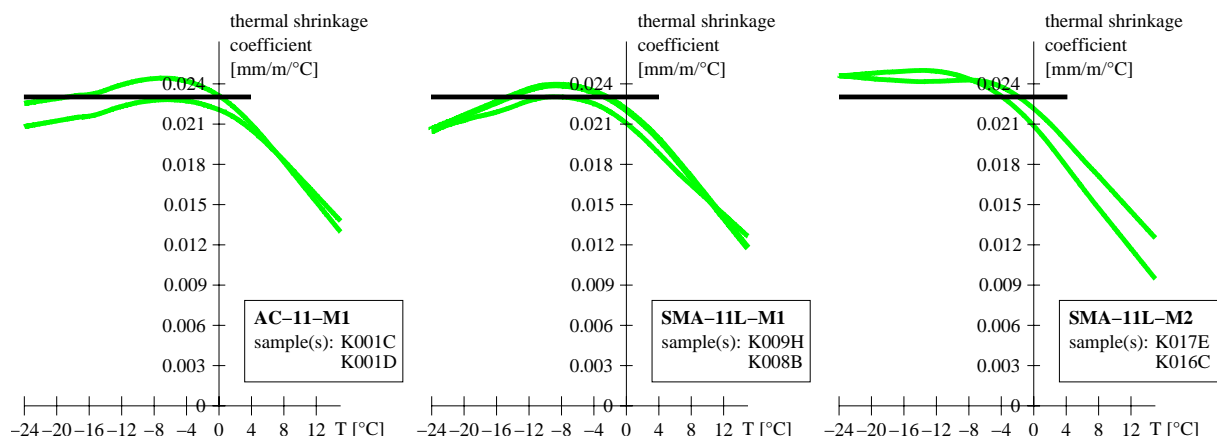


Figure 3: TST results: thermal shrinkage coefficient  $\alpha_T$  [mm/m/°C] as a function of temperature.

#### 4.2 Results from Uniaxial-Tensile-Strength Tests (UTSTs)

Whereas the TST provides insight into the loading of asphalt layers when subjected to temperature drops, the UTST gives its resistance to fracture. UTSTs are standardly performed by applying a constant displacement rate of 1 mm/min, giving for the case of specimen lengths of 225 mm a strain rate of 267 mm/m/h. This strain rate, however, exceeds the strain rate during in-service situations with temperature cooling rates up to  $10\text{ }^\circ\text{C/h}$  and, thus, thermal strain rates of  $10 \times 0.023 = 0.23\text{ mm/m/h}$ , by a factor of 1000! In order to assess the influence of the strain rate on UTST results, tests were conducted with strain rates of 1 mm/min and 0.1 mm/min. In Figure 4, the effect of the strain rate is illustrated for two test

temperatures, namely -10 °C and -25 °C. Whereas the strain rate hardly influences the stress-strain relation and, thus, the tensile strength at a test temperature of -25 °C, the material response is significantly different at -10 °C. Using the lower strain rate, redistribution of the microstress in the bitumen results in the development of slip planes, leading to a zero-stiffness failure (almost horizontal tangent at failure) corresponding to materials failing under Mode II. At the original strain rate (with a displacement rate of 1 mm/min), Mode I (brittle) failure is observed.

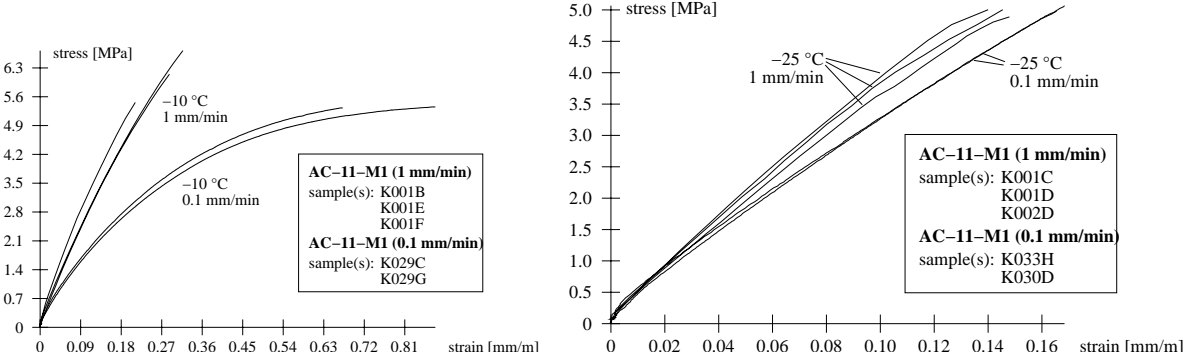


Figure 4: UTST results: influence of displacement rate on stress-strain relation and tensile strength.

Figure 5 shows UTST results for the considered asphalt mixtures for a test temperature of -10 °C. Even though the same displacement rate (1 mm/min) was used for all experiments, the different viscous behavior results in Mode I failure for AC-11-M1, in Mode II failure for SMA-11L-M2 (with pmB as binder material), and in mixed mode failure for SMA-11L-M1. In contrast to the TST, where air voids did not influence the obtained results, air voids trigger crack initiation and, thus, strongly influence the tensile strength: the higher the amount of air voids, the lower the tensile strength. The higher values for the tensile strength of the SMA-11L-M2 (when compared to the results obtained for SMA-11L-M1, both having the same amount of air voids) is explained by the better low-temperature performance of pmB. This positive effect of the pmB even increases for lower test temperatures.

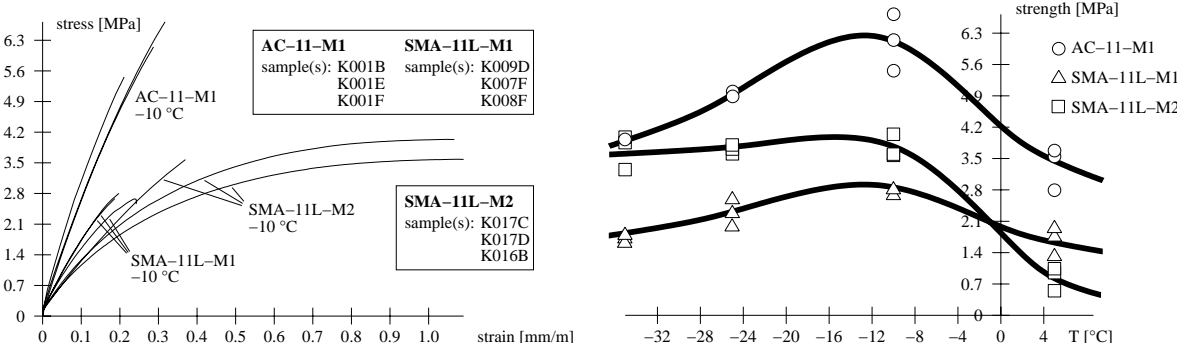


Figure 5: UTST results: stress-strain relation and tensile strength for considered asphalt mixtures (displacement rate = 1 mm/min).

### 4.3 Results from Creep Tests (CTs)

The creep tests are performed in order to study the viscous behavior of asphalt, which was found to influence the TST results at above-zero temperatures and the tensile load-carrying

behavior even at sub-zero temperatures (see Figures 3 and 4). For the interpretation of CT results, the monitored strain history is related to the applied (constant) stress, giving the so-called creep compliance  $J(t) = \text{strain}(t)/\text{stress}$ . The creep compliance obtained from CTs of AC-11-M1 performed at different temperatures are shown in Figure 6. The derivation of the creep compliance with respect to time yields the creep compliance rate  $dJ/dt$  depicted in Figure 6. The linear relation found in the  $\log_{10} dJ/dt - \log_{10} t$  diagram reveals that creep of asphalt under tensile loading is a declining, but not an asymptotically declining process, following a power-law in the form  $dJ/dt = H (t/\tau)^p$ , where  $\tau$  is a dimensional constant, with  $\tau = 1$  s. From a material-modeling point of view, this fact is commonly considered by the consideration of a nonlinear dashpot, representing exactly this type of creep behavior.

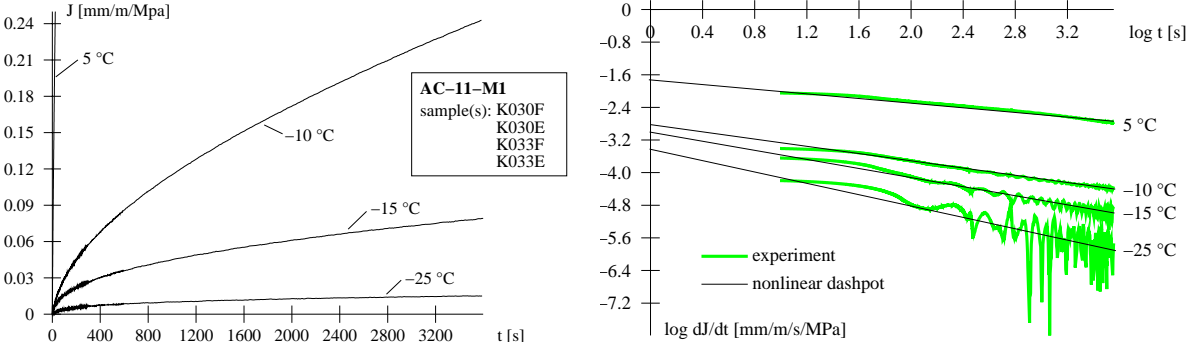


Figure 6: CT results: creep compliance  $J$  and creep compliance rate  $dJ/dt$  for AC-11-M1 for different temperatures.

Plotting the obtained values of the parameters  $H$  and  $p$  as a function of temperature, relations already found from low-temperature testing of bitumen and mastic (bending beam rheometer, see (Lackner et al. 2005)) are recovered. E.g., the Arrhenius law used to describe the influence of the temperature on the creep parameter  $H$  gives an activation-energy/gas-constant ratio of 9000 K, the same value as reported in (Lackner et al. 2005) for pure bitumen. Thus, the creep behavior of asphalt under tensile loading is mainly controlled by the properties of the binder material. In contrast to creep under compressive loading, the contact between aggregate grains and aggregate interlock are of minor importance.

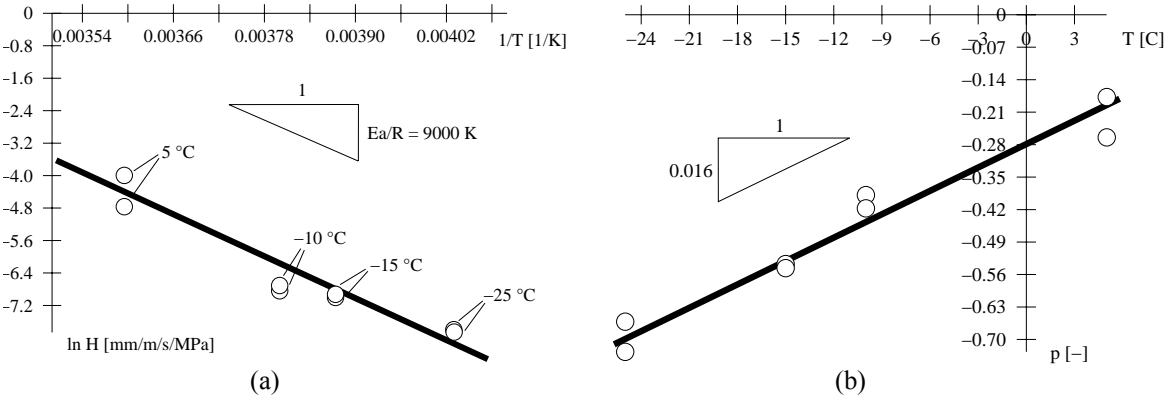


Figure 7: CT results: creep parameters  $H$  and  $p$  as a function of the temperature for AC-11-M1.

#### 4.4 Results from Relaxation Tests (RTs)

Whereas the CTs were performed for the specification of the viscous properties of asphalt under constant external loading, the material stiffness is obtained from RTs. After the application of a strain increment  $\epsilon_0$  which, thereafter, is kept constant throughout the RT, viscous processes are driven by the material stiffness resulting in stress relaxation. Extending the already identified power-law creep model (nonlinear dashpot, parameters  $p$  and  $H$ ) by a linear spring (connected in series), the stress history associated with RTs is obtained from

$$\dot{\epsilon}(t) = \dot{\epsilon}^{ve} = \dot{\epsilon}^e + \dot{\epsilon}^v = \frac{\dot{\sigma}(t)}{E} + \frac{dJ}{dt}\sigma(t) = \frac{1}{E}\dot{\sigma}(t) + H\left(\frac{t}{\tau}\right)^p \sigma(t) = 0 \quad (2)$$

giving

$$\sigma(t) = \sigma_0 \exp\left[-\frac{EH}{p+1}\left(\frac{t}{\tau}\right)^{p+1}\right], \quad (3)$$

where  $E$  is the stiffness of the linear spring and  $\sigma_0$  represents the stress right after application of the strain increment  $\epsilon_0$ . Figure 8 shows the stress histories obtained from the RTs and the respective model prediction corresponding to Equation (3), where the creep parameters  $H$  and  $p$  were taken from Figure 7 and the yet unknown parameter  $E$  was identified. From the obtained results, the following conclusions can be drawn:

- Since the elastic parameter  $E$  influences only the time scale of the relaxation process (see Equation (3)), perfect fit between the experimental results and the model response was achieved by using a reduced value for the initial stress  $\sigma_0$ . This decrease as well as the deviation of the model response from the experimental data in the first 100 seconds is explained by the disregard of short-term creep deformation, which would have required consideration of a second nonlinear dashpot connected in series, finally giving the so-called Huet model.
- Moreover, the employed model, characterized by a linear spring and a nonlinear dashpot in series, would result in stress relaxation towards zero-stress. The remaining residual stress observed in the RTs is taken into account by reformulating Equation (3) in the form

$$\sigma(t) = \sigma_\infty + (\sigma_0 - \sigma_\infty) \exp\left[-\frac{EH}{p+1}\left(\frac{t}{\tau}\right)^{p+1}\right], \quad (4)$$

suggesting the existence of a second spring, with stiffness  $\sigma_\infty/\epsilon_0$ , connected in parallel, as found in the so-called Huet-Sayegh model.

The so-obtained parameters for the performed RTs are listed in Table 3.

Table 3: Model parameters obtained form RTs.

sample	T [°C]	$\epsilon_0$ [mm/m]	$\sigma_0$ [MPa]	E [MPa]	$\sigma_\infty$ [MPa]
109E	5	0.112	0.99	1100	0.03
K003B	-10	0.042	1.56	23000	0.35
112C	-15	0.056	1.63	17000	0.28
K031G	-25	0.043	1.43	25000	0.19

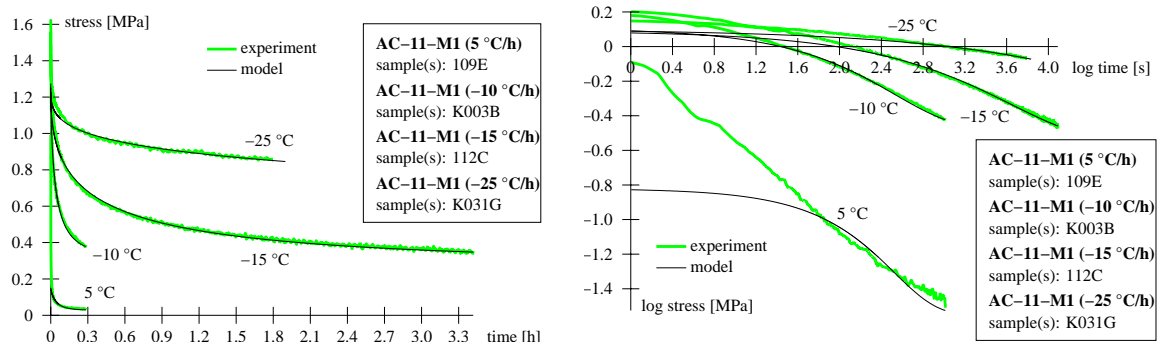


Figure 8: RT results: stress history for AC-11-M1 for different temperatures.

#### 4.5 Results from Tensile-Stress-Restrained-Specimen Tests (TSRSTs)

With the obtained background in characterization of low-temperature behavior of asphalt at hand, finally TSRSTs were performed. Figure 9 shows the thermally-induced stresses as a function of the specimen temperature for two different cooling rates (SHRP, 1994). In accordance to the observed impact of the temperature on the stress-strain relation for temperatures higher than -15 °C (see UTST results), the main deviation caused by the different cooling rates develops during cooling to -15 °C. From this temperature until failure, an almost similar material response is encountered, stemming from mainly elastic material behavior. In case of elastic material behavior, the continuous decrease of  $d\sigma/dT$  suggest, that the elastic material properties change with temperature. Otherwise, the stress increase would have followed the induced thermal strains, with  $d\sigma/dT$  directly related to the thermal shrinkage coefficient which, for decreasing temperature, was found to decrease slightly, while the absolute value of  $d\sigma/dT$  further increases.

Specimen failure itself seems to be independent of the cooling rate, as failure occurs at temperatures where the influence of the temperature on the tensile strength was found to be marginal (see, e.g., UTST results for -25 °C).

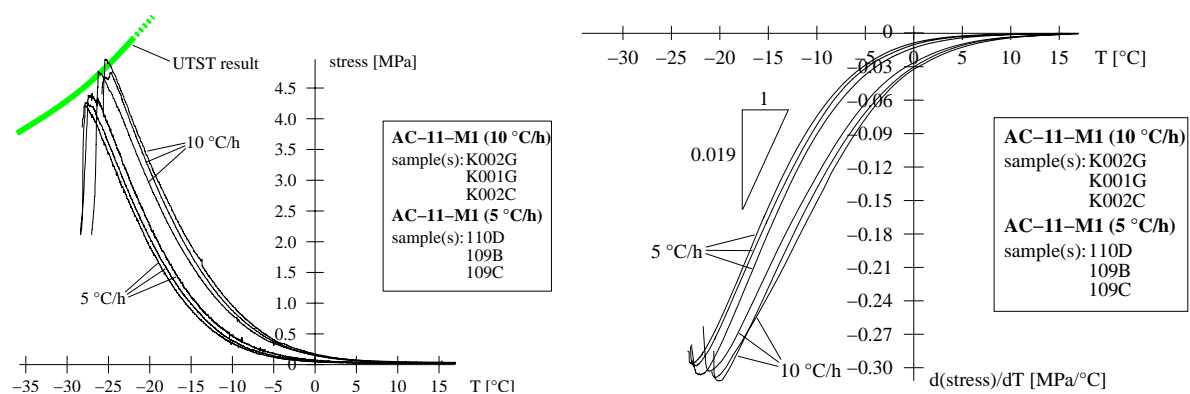


Figure 9: TSRST results: effect of cooling rate on experimental results.

The comparison of TSRST results in Figure 10 for the investigated asphalt mixtures reveals the low relaxation capacity of AC-11-M1, even though a softer standard bitumen was used. The significant stress build-up with decreasing temperature results from the low amount of air voids with 3 vol-%, explaining both the high viscosity and the rather high fracture stresses of up to 4.5 MPa already observed in the UTST results. The higher amount of air voids within the SMA-11L mixtures provides more mobility for aggregate particles to re-arrange, resulting

in a higher stress-relaxation capacity. This effect is even higher for SMA-11L-M2, with pmB as binder material. The pmB is characterized by a lower viscosity in the low-temperature range and, as known from testing of pure pmB, exhibits a higher tensile strength than standard bitumen.

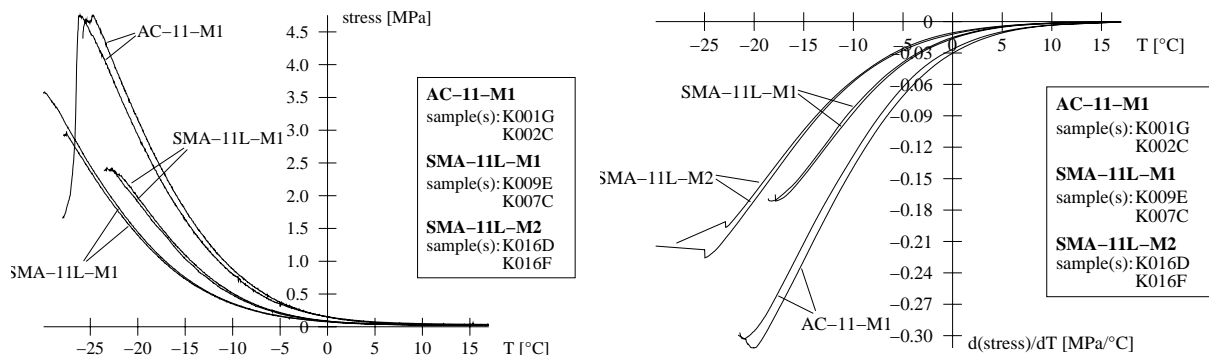


Figure 10: TSRST results: effect of asphalt mixture on experimental results (cooling rate = 10 °C/h).

## 5 CONCLUDING REMARKS AND OUTLOOK ON FUTURE WORK

In this paper, a set of test methods was presented for characterization of the low-temperature performance of asphalt mixtures. More specifically, the commonly used TSRST was reviewed as regards reproducibility of experimental results, the influence of test parameters, and the physical soundness of key material parameters such as e.g. the tensile strength reserve. From the obtained results, the following conclusions can be drawn:

- The good reproducibility of experimental data, as shown in the results presented in this paper, strongly depends on the preparation and quality of the asphalt plates (length x width x height = 500 x 260 x 50 mm) from which the prismatic test specimens were obtained by cutting. For the preparation of these plates, the hot asphalt was filled into the segment roller compactor in a uniform way, aiming at an equal distribution of the asphalt mass. Furthermore, prismatic specimens exhibiting damage, such as cracks on the specimen surface, or agglomeration of large-size aggregate grains in one part of the specimen were excluded from the test program. Moreover, each specimen, when approved for testing, was mounted onto the steel adaptors by a two-component glue which was placed on the adaptor itself and on the side faces of the specimen close to the adaptor-specimen interface. This mode of mounting resulted in crack initiation and failure of specimens in the center area of the specimens, i.e., in an area characterized by a homogeneous stress state, sufficiently far away from the adaptors.
- The test parameters for the TSRST and the UTST were found to considerably influence the experimental results. E.g., a change of the cooling rate for TSRSTs resulted in a shift of the stress-temperature relation, giving different values for the fracture stress and the fracture temperature for the same type of asphalt. However, in case of a defined test procedure using only one cooling rate, these parameters may be used to compare the performance of different asphalt mixtures in the low-temperature regime. The tensile strength reserve, on the other hand, is obtained from combining TSRST and UTST data, where for the latter a significant influence of the loading rate was encountered. Taking the influence of the loading rate on UTST data and the mentioned influence of the cooling rate on TSRST data into account, the tensile

strength reserve provides only a qualitative measure for the low-temperature performance of asphalt mixtures. It does not provide quantitative information regarding e.g. the level of loading or the risk of fracture at a certain temperature.

In addition to the assessment of key material parameters describing the low-temperature performance of asphalt mixtures, the performed tests provided useful information on the thermorheological and fracture behavior of asphalt. E.g., the TST results indicated an almost constant value for the thermal shrinkage coefficient in the negative temperature regime, with  $\alpha_T$  approximately 0.023 mm/m/°C for all considered types of asphalt. The results from CTs and RTs can be used for both the development of appropriate viscoelastic material models and the identification of the respective model parameters.

In order to solve the encountered discrepancy between CTs and RTs – the CT results agreed well the response of the so-called power-law, while the RT results required the consideration of an additional spring connected in parallel – micromechanical approaches, taking several observation scales into account, are currently developed. Future work will focus on upscaling of “macroscopic” model parameters from finer observation scales in order to relate the thermomechanical behavior of asphalt to the behavior of the asphalt constituents and their arrangement (Lackner et al. 2004).

In the same line, the tensile strength of asphalt (requiring time-consuming UTSTs) will be related to the behavior of the binder material. First promising results obtained from SHRP Direct Tension Tests (DTTs) on bitumen (mastic) and UTSTs on asphalt are shown in Figure 11. In addition to the experimental work, the aforementioned multiscale approach will be employed to relate strength properties determined experimentally at different scales of observation (DTT-strength at the *bitumen*- and *mastic*-scale and UTST-strength at the *mortar*- and *asphalt*-scale).

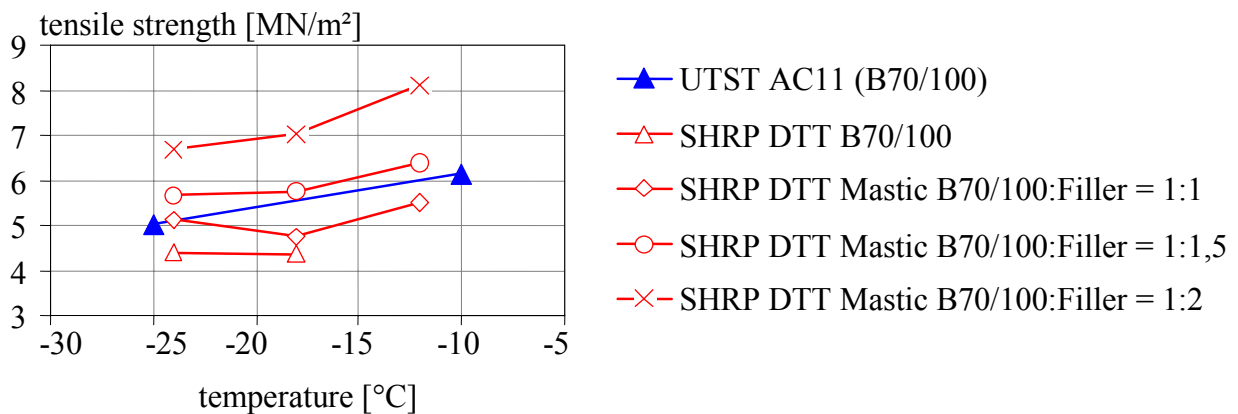


Figure 11: Comparison of tensile strengths obtained from DTT binder testing and UTST testing of asphalt.

In a further step these different test methods will be used to formulate reliable optimization parameters, i.e. key material characteristics of bituminous bound materials to describe low temperature behavior on the basis of a lower performance grade that subsequently can be incorporated in a performance based mix design procedure.

## ACKNOWLEDGEMENT

Financial support by the Christian Doppler Forschungsgesellschaft (Vienna, Austria) is gratefully acknowledged. The authors thank Georg Schiner for the conduction of the experiments and Josef Füssl for helpful support during interpretation and post-processing of experimental data.

## REFERENCES

- Arand, W., Steinhoff, G., Eulitz, J. und Milbradt, H. 1984. *Verhalten von Asphalten bei tiefen Temperaturen; Entwicklung und Erprobung eines Prüfverfahrens*. Schriftenreihe „Forschung Straßenbau und Straßenverkehrstechnik“ des Bundesministers für Verkehr, Abteilung Straßenbau, Heft 407, Bonn-Bad Godesberg, Deutschland.
- FGSV - Forschungsgesellschaft für Straßen- und Verkehrswesen, Arbeitsgruppe Asphaltstraßen. 1994. *Technische Prüfvorschrift - Verhalten von Asphalten bei tiefen Temperaturen*. FGSV 765. In German.
- Lackner, R., Blab, R., Jäger, A., Spiegl, M., Kappl, K., Wistuba, M., Gagliano, B., and Eberhardsteiner, J. 2004. *Multiscale modeling as the basis for reliable predictions of the behavior of multi-composed materials*. Progress in Engineering Computational Technology, Chapter 8, 153-187, Saxe-Coburg Publications, ISBN 1-874672-22-9.
- Lackner, R., Spiegl, M., Blab, R., and Eberhardsteiner, J. 2005. Is Low-Temperature Creep of Asphalt Mastic Independent of Filler Shape and Mineralogy? – Arguments from Multiscale Analysis. *Journal of Materials in Civil Engineering (ASCE)*. In print.
- Olard, F. 2003. Comportement thermomécanique des Enrobés bitumineux à basses températures. Relations entre les propriétés du liant et de l'enrobé. Département Génie Civil et Bâtiment, Ecole Nationale des TPE. In French.
- Pichler, Ch., Lackner, R., and Mang, H.A. 2003. Continuum-micromechanics approach for determination of frost heave in artificial ground freezing. Proceedings of the 2nd MIT Conference on Computational Fluid and Solid Mechanics (ed.: Bathe, K.J.). 578-581, Elsevier Science Ltd., Oxford.
- SHRP - Strategic Highway Research Program. 1994. *Low-Temperature Cracking: Field Validation of the Thermal Stress Restrained Specimen Test*. (SHRP-A-401). National Research Council, Washington DC.
- Spiegl, M., Wistuba, M., Lackner, R. and Blab, R. 2005. *Risk assessment of low-temperature cracking of asphalt – an experimental study*. Proceedings of 11<sup>th</sup> International Conference on Fracture, Turin, Italy, March 20-25. In print.
- Wistuba, M. 2002. *Klimaeinflüsse auf Asphaltstraßen: Maßgebende Temperatur für die analytische Oberbaubemessung in Österreich*. Mitteilungen des Instituts für Straßenbau und Straßenerhaltung, Heft 15, Vienna University of Technology, Austria. In German.